ROTOR BLADE DESIGN FOR A COAXIAL HELICOPTER IN MARTIAN ATMOSPHERE IN HOVER AND FORWARD FLIGHT

Stefan Hönes
Research Associate

İlkay Yavrucuk
Professor

Institute for Rotorcraft and Vertical Flight
Technical University of Munich
Munich, Germany

ABSTRACT

This paper outlines the design process of rotor blades of a Martian coaxial unmanned aerial vehicle (UAV) designed to scout the Valles Marineris for subsequent exploration by rovers. The low atmospheric density causes performance degradation of conventional airfoils and lower aerodynamic damping [8]. This necessitates performance optimized, lightweight rotor blades with high stiffness. The paper presents the aeromechanic mid-fidelity CAMRAD II model [4] to assess the rotor blade performance and the following design process for of the rotor blades. Different rotor platforms are compared to serve as baseline for the following optimization for forward flight. To reduce the dominating profile power, the chord length of the blade was reduced at the tip and increased towards the centre, which led to savings in the total power of 3.17 %. Twist has been reduced in comparison to a hover optimized blade to -7.5 degrees linear twist.

NOTATION

*

Symbols

a Speed of Sound, $\mathrm{m\,s^{-1}}$

g Gravitational acceleration, $\mathrm{m\,s^{-2}}$

n_{Blade} Number of blades

n_{Rotor} Number of rotors

$m_{Payload}$ Payload mass, kg

P Pressure, Pa

P_i Induced power, kW

r_{Rotor} Rotor radius, m

R Maximum rotor radius, m

T Temperature, K

V_{cruise} Cruising speed, $\mathrm{m\,s^{-1}}$

ρ Density, $\mathrm{kg\,m^{-3}}$

η Dynamic viscosity, $\mathrm{Pa\,s}$

*

Acronyms

AE Aerial Explorer

AREA Autonomous rotorcraft for extreme altitudes

DGOW Design Gross Weight

DL Disk Loading

DLR German Aerospace Center

FM Figure of Merit

LE Leading Edge

MH Mars Helicopter

NASA National Aeronautics and Space Administration

NDARC NASA Design and Analysis of Rotorcraft

TE Trailing Edge

TUM Technical University of Munich

UAV Unmanned Aerial Vehicle

VaMEx Valles Merineris Explorer

INTRODUCTION

Following the success of the Ingenuity Mars Helicopter in 2021, UAVs promise to be a powerful tool in the exploration of extraterrestrial bodies. As part of the German Aerospace Center's (DLR) Valles Marineris Explorer (VaMEx) initiative to explore Mars by means of a swarm of rovers, an Martian UAV is being developed at the Technical University of Munich (TUM) to support this swarm by mapping the region around the lander and identifying points of interest [15]. In the scope of this project, the preliminary design of the UAV has been completed and special rotor blades have been developed, that will be manufactured and tested in an planned in-house vacuum chamber to test them under Martian conditions. The low atmospheric density causes a high degradation in the performance of conventional airfoils and thus the rotor blade, as well as aerodynamic damping [8]. This necessitates performance optimized, light weight rotor blades with high stiffness. Previous research, mainly conducted by Koning and Johnson et al [7, 11] focused on the design of small rotor blades, with radii of around 0.604 m and 0.64 m respectively [7]. Both feature hover optimized rotor blades with. This paper covers the design process for larger rotor blades with a radius of 1.52 m, which are optimized for forward flight. The results of this blade design and the following testing campaign under simulated Martian conditions serve as a basis for the future development of bigger rotorcraft for Mars to allow a higher ranges and potentially higher payload.

The paper presents the aeromechanic model that was created with the mid-fidelity, aeromechanical analysis software CAMRAD II [4] to assess the rotor blade performance as well as the fulfilment of the design requirements. After the model and verification are introduced, the blade design itself is discussed. This includes an adaption of the rotor chord length for forward flight, twist distribution, as well as the rotor blade root and structural design. The developed rotor blades will serve as a test platform to validate the aeromechanic model and generate test data for future designs.

MISSION

The proposed UAV is developed as part of the subproject VaMEx-Aerial Explorer (AE). The goal of this initiative is the autonomous exploration of Valles Marineris, through the coordinated deployment of a swarm consisting of rovers, crawlers, and a UAV. Due to its lower altitude and thus higher pressure, this region promises signs of water and is therefore interesting for further exploration [1].

The task of the UAV is to explore the area surrounding the lander and identify scientifically relevant points of interest for subsequent investigation by the ground-based rovers and crawlers [1].

The lander functions as both a communications relay and a charging hub. Hence, the UAV is not equipped with solar panels and relies entirely on energy supplied by the lander. The mapping and data acquisition tasks are carried out during the cruise phase. Thus, hovering is only required for take-off and landing, minimizing the need for prolonged stationary flight. The UAV accelerates and decelerates during climb and descent, decreasing hover time and making cruise the primary mission segment. Thereby, the UAV must be capable of completing a return mission with an operational radius of 14 km, resulting in a total mission distance of 28 km. To provide a design margin, a maximum range of 30 km was set [15].

REQUIREMENTS AND BOUNDARY CONDITIONS

The design requirements of the rotor blades are derived from both the UAV configuration and the environmental conditions on Mars. The operational constraints of the mission necessitate an optimization of the UAV and the rotor blades for forward flight with a previously defined velocity of 40 m/s. The total cruise phase is estimated to last about 0.2 h, compared to an estimated hover time of 40 s. This is based on empirical data of terrestrial UAV configurations designed for similar mission profiles [15].

The payload capacity, including navigation systems, scientific instrumentation, telemetry, and onboard electronics, is approximately 2.2 kg [15].

Two potential configurations were evaluated, with a coaxial rotor system ultimately selected as the most suitable option [15]. The configuration is depicted in Figure 1.

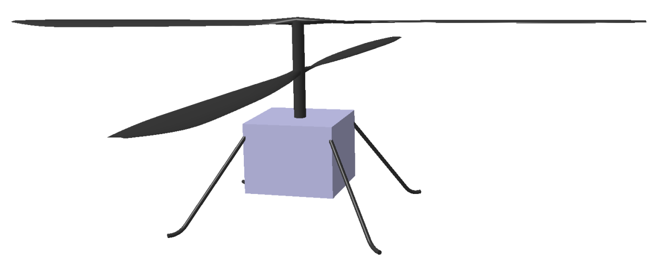

Figure 1: Coaxial helicopter configuration [15].

A sizing loop was performed using the aircraft system analysis tool NDARC [6] to determine the UAV's parameters relevant to rotor blade design [15]. The results are presented in Table 1. A rotor radius of 1.52 m and a disk loading of $5.5\ \mathrm{N/m^2}$ were obtained, which defined the required rotor blade solidity and plan-form area.

In addition, the Martian environment imposes aerodynamic and structural constraints. The Martian atmosphere is composed of approximately 95 % carbon

Table 1: VaMEx Mars Helicopter key design parameters [15].

Parameter	Symbol	Value
Rotor Radius	r_{Rotor}	1.52 m
Number of Rotors	n_{Rotor}	2
Number of Blades	n_{Blade}	2
Disc Loading	DL	5.5 $\mathrm{N\,m^{-2}}$
Rotational Speed	RPM	1162 $\mathrm{min^{-1}}$
Weight	$DGOW$	21.5 kg
Payload Mass	$m_{payload}$	2.2 kg
Cruising Speed	V_{cruise}	40 $\mathrm{m\,s^{-1}}$
Range	$Range$	30 km

dioxide (CO_2) and is characterized by a lower mean surface air density and temperature than those on Earth [13]. The average atmospheric density is approximately 0.02 $\mathrm{kg/m^3}$, which amounts to less than 2 % of Earth's mean sea-level density. However, these parameters vary widely, with the ambient temperature fluctuating by up to 60 K per day [14]. This influences the lift capability of the rotor blades. In contrast, the gravitational acceleration on Mars is 3.71 $\mathrm{m/s^2}$ (approximately 38 % of Earth's), which benefits the UAV's performance [7].

For the design process, a representative atmospheric design point from the Valles Marineris region was selected. This location features relatively higher average temperatures and approximately 10 % greater atmospheric density compared to the Martian surface mean, which benefits the lift capabilities. The temporal variations in temperature, as well as the effects of wind and gusts, were not considered in the design. A comparative summary of atmospheric conditions on Earth, Mars, and Valles Marineris is provided in Table 2 [3, 14].

The low atmospheric density also results in lower Reynolds numbers and shifts the airfoil's minimum drag characteristics. Additionally, the reduced speed of sound in the Martian atmosphere imposes further limitations on the rotor's rotational speed, resulting in a final speed of 1162 rpm [15].

Table 2: Atmospheric conditions on Earth, Mars surface and Valles Marineris (VM) [3, 14].

		Earth	Mars	VM
Grav. acc g	$[\mathrm{m\,s^{-2}}]$	9.81	3.71	3.71
Temp. T	[K]	288	210	218
Pressure p	[Pa]	101325	636	895
Density ρ	$[\mathrm{kg\,m^{-3}}]$	1.225	0.02	0.022
Dyn. visco. η	$[\mathrm{kg\,m^{-1}\,s^{-1}}]$	1.7	1.1	1.1
Sound speed a	$[\mathrm{m\,s^{-1}}]$	340	233	235

MODELLING

For the analysis of potential rotor blade geometries, an aeromechanical model is developed. This model serves to simulate the flight characteristics of the field-test demonstrator and as the analytical foundation for evaluating blade designs. The simulation is implemented using CAMRAD II.

The model is created and validated based on data from [10]. It represents the coaxial rotor system, excluding the UAV fuselage, and assumes a free-flight configuration. Due to the dimensional disparity between the helicopter in [11] and the VaMEx Mars Helicopter, direct validation is not feasible. To address this, a model of [11] was first created, with adjusted rotor size and rotational speed and validated against experimental data. This validated model was subsequently scaled up to the desired radius and rpm, and the structural model of the blades was changed from rigid to elastic. This approach preserves physical consistency within the simulation. Complete validation and evaluation will only be possible upon completion of a planned rotor test campaign under a simulated Martian atmosphere.

Baseline Model

The baseline model builds upon a previously developed CAMRAD II uniform inflow model of a Martian coaxial helicopter, originally created during the preliminary UAV design study presented in [15]. The uniform inflow model uses empirical models based on momentum or vortex theory. It was modified to a non-uniform inflow, free wake geometry model. The non-uniform inflow calculates the induced velocity from an integral equation, and the free wake geometry calculates the wake geometry based on this, instead of using a prescribed or empirical wake [4]. This enhances the accuracy of the model, which is particularly relevant for the lower rotor. It is based on the rotor parameters of the helicopter, as detailed in[9], with a rotor radius of 0.605 m and 2600 rpm. This configuration enables validation against both experimental data and simulation results presented in [11].

In this baseline configuration, rotor blades are assumed to be rigid. While this may lead to overestimation of aerodynamic forces, it improves the numerical stability. A model incorporating elastic blades will be developed in a subsequent phase to enable the study of structural dynamics and the generation of better force predictions.

Verification The verification is based on the available data in [11], mainly the presented plot of Figure of Merit over blade loading (C_T/σ). It shows the comparison between the test data and the CAMRAD II simulation results. To replicate the Figure of Merit (FM) across a range of blade loadings, the vehicle is analysed in hover and the weight is incrementally increased from 0.7 kg to 1.2 kg. The resulting data is compared with reference values shown in Figure 2. Environmental parameters have been aligned with those presented in [10]. These parameters are listed in Table 3. Since the tests were conducted under the influence of Earth's gravity and without an offloading system in place, a gravitational acceleration of 9.81 $\mathrm{m\,s^{-2}}$ is used.

Table 3: CAMRADII environmental settings for baseline model verification [10].

Density	ρ	0.017 $\mathrm{kg\,m^{-3}}$
% Speed of Sound	a	233.13 $\mathrm{m\,s^{-1}}$
Temperature	T	223 K

Figure 2, includes CAMRADII results from Koning et al. [11] and the present simulation results from TUM.

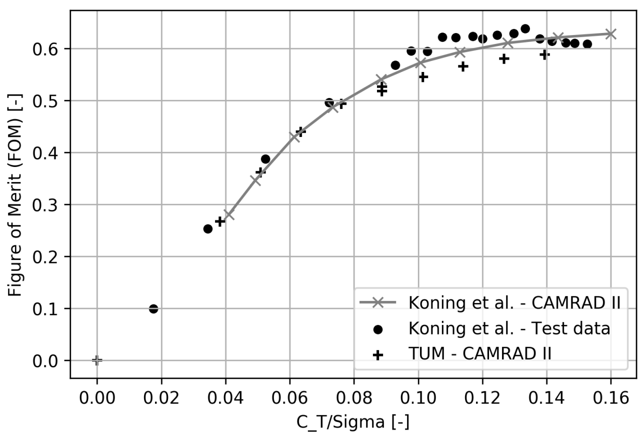

Figure 2: Comparison of CAMRAD II simulation results with test data and simulations from [12]

The figure shows the comparison between test data (black dots) and CAMRAD II simulations (grey line) from Koning et al. [11], and the TUM results (black crosses). Both replicate the trend of the test data well, and good agreement is observed up to a C_T/σ value of approximately 0.09, beyond which the TUM model under predicts the Figure of Merit. Equation 1 shows the correlation between induced-, ideal induced-, and profile power.

$$FM = \frac{P_{Ideal}}{P_{real,Ideal} + P_{Profile}} \tag{1}$$

P_{Ideal} and $P_{Profile}$ are functions of Thrust, Area, Density, and the drag coefficient. All of which are given by the airfoil data and geometry provided in [9]. Therefore, the difference in magnitude is most likely arising in the calculation of the real induced power. This suggests that the wake models are not completely identical and the wake losses are over predicted, which results in a higher $P_{real,Ideal}$ and a lower FM. Nevertheless, the deviation remains within acceptable bounds and is consistent with trends seen in the NASA CAMRAD simulations.

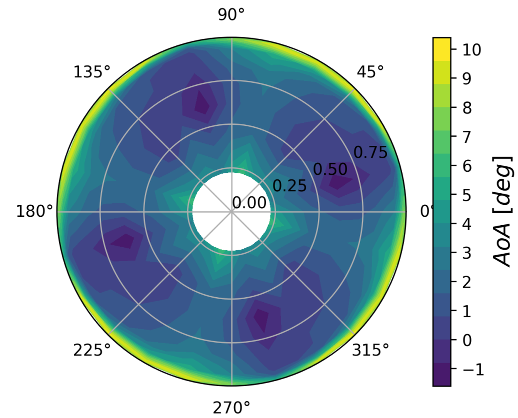

(a) Lower rotor (Rotor 1).

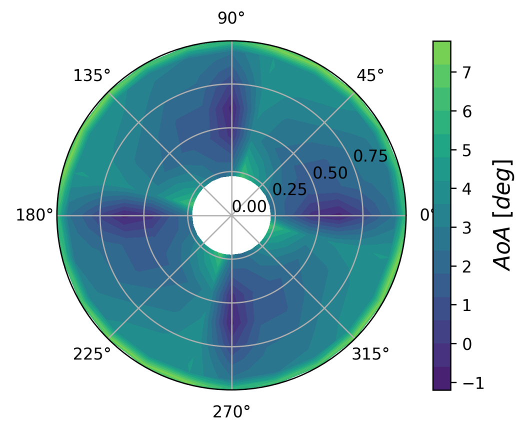

(b) Upper rotor (Rotor 2).

Figure 3: Angle of attack distribution for the upper and lower rotor in hover.

Physical Verification To verify the physical plausibility of the simulation, the angle-of-attack distributions across the rotor disks were evaluated, see Figure 3. In hover, a uniform inflow and hence uniform angle-of-attack distribution is expected for the upper rotor of the coaxial configuration. The lower rotor is affected by the downwash of the upper rotor and hence is expected to have an increased mean angle of attack. Also, the effect of the rotor blades and the stream tube contraction is expected to be visible in the disk plots. Due to the contraction of the stream tube below the upper rotor, the effect on the lower rotor is spatially confined to the inner regions, whereas the outer region shows a higher angle of attack. In regions where the rotor blades cross each other, a change in angle of attack is also expected. This results in a symmetric but not uniform distribution.

As depicted in Figure 3, the angle of attack distribution is symmetric but not uniform. This non-uniformity arises from blade–wake interactions and is expected in coaxial configurations. Due to the induced velocity of the upper rotor, the mean angle of attack for the lower rotor is reduced compared to the upper rotor, particularly within the inner radial region ($r/R < 0.85$). Beyond this region, the downwash influence is lower due to the stream tube contraction. These observations are consistent with expectations.

The model trim settings are also evaluated. Since all test cases simulate the aircraft in hover, only collective and yaw inputs are expected, while cyclic and longitudinal control inputs should remain zero. A small yaw input is anticipated due to thrust asymmetry between the two rotors, see Table 4.

Table 4: Control inputs in trimmed hover configuration.

Control Input	Value
Collective	7.459
Lateral Cyclic	0.356×10^{-3}
Longitudinal Cyclic	-0.505×10^{-3}
Yaw	0.609
Pitch	-0.385×10^{-3}
Roll	-0.520×10^{-4}

The control input values confirm the expected behaviour. Only collective and yaw commands exhibit significant magnitudes, with the latter compensating for torque imbalance due to asymmetric rotor loading. Cyclic and trim inputs are negligible, as anticipated under symmetric hover conditions.

This concluded the verification of the model. The results were deemed physically consistent and aligned with available reference data, validating the use of this configuration as a baseline for subsequent upscaling.

Scaled Free-Wake Model

The rotor geometry was updated to reflect the VaMEx Mars Helicopter. Environmental conditions were modified to match those at Valles Marineris. The updated model underwent numerical and physical verification. Due to a lack of experimental data for this configuration, direct validation is not possible; it will be conducted upon completion of the planned test campaign.

For numerical validation, relaxation factors, convergence tolerances, and blade/vortex discretization settings were systematically varied to evaluate their impact on convergence. These parameters were selected based on prior modelling experience.

The evaluation focused on convergence behaviour and solution robustness. Since the model is intended for iterative optimization, rapid convergence is desirable, but must not compromise numerical stability, especially under low blade-loading conditions.

The analysis revealed convergence challenges at near-zero blade loads.

The numerical verification confirmed that the model is sufficiently robust across most of the intended flight envelope and is suitable for design analysis.

The rotor model was upgraded to include elastic blades, enabling the simulation of structural dynamic effects. The updated model was subjected to the same verification process and successfully passed all verification steps.

BLADE DESIGN

The blade design started with the aerodynamic design and continued with the structural design. The process begins with selecting the airfoil for low Reynolds numbers. The geometry of the rotor blade, its twist and the transition to the blade root are designed subsequently.

Airfoil Selection

The airfoil selection was based on data from [12]. The paper examined the efficiency of different airfoils, which are shown in Figure 4.

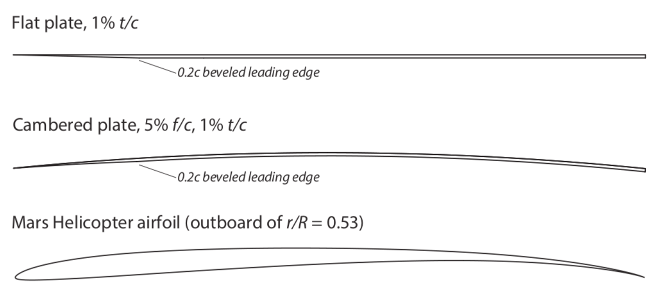

Figure 4: Potential airfoils for the VaMEx Mars Helicopter [12].

The best results were achieved using thin, cambered airfoils. This promised an increase in Figure of Merit over the entire blade loading range with a peak of around 5 % and an increased maximum thrust of 7 % compared to the Mars Helicopter airfoil (CLF5605) [12]. The profiles and the comparison of the Figure of Merit are shown in Figures 5.

However, it was expected that the low thickness of the cambered airfoils would lead to structural problems with larger blades. This is based on the findings of Johnson and Fj et al. [2, 7] that showed that the lack of aerodynamic damping requires blades with high stiffness. For this reason, thin airfoils were excluded from further design considerations.

The Mars Helicopter profile CLF5605 was selected as an alternative. It has a significantly greater thickness and promises better results for the structure, with acceptable values for aerodynamic efficiency.

Chord Distribution

Using the rotor radius and disc loading from Table 1, the required blade area was determined and amounts

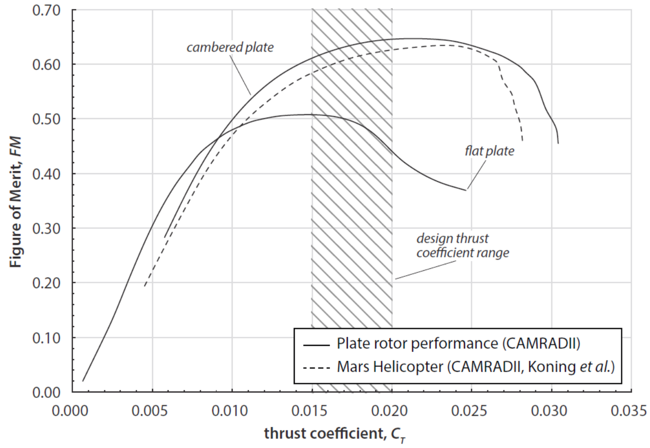

Figure 5: Figure of Merit comparison between cambered plate airfoil and Mars Helicopter blade [12].

to 0.52 m^2. The selected geometries were based on existing geometries for Martian UAVs, as well as high-altitude drones. The comparison includes rotor blades from NASA's Ingenuity helicopter and the Mars Science Helicopter (MH), an in-house developed AREA blade, and a standard rectangular blade. They are depicted in Figure 6. Although the AREA blade was not initially intended for Martian operation, its similar rotor radius (1.65 m) and high-altitude design characteristics rendered it a suitable candidate for this study.

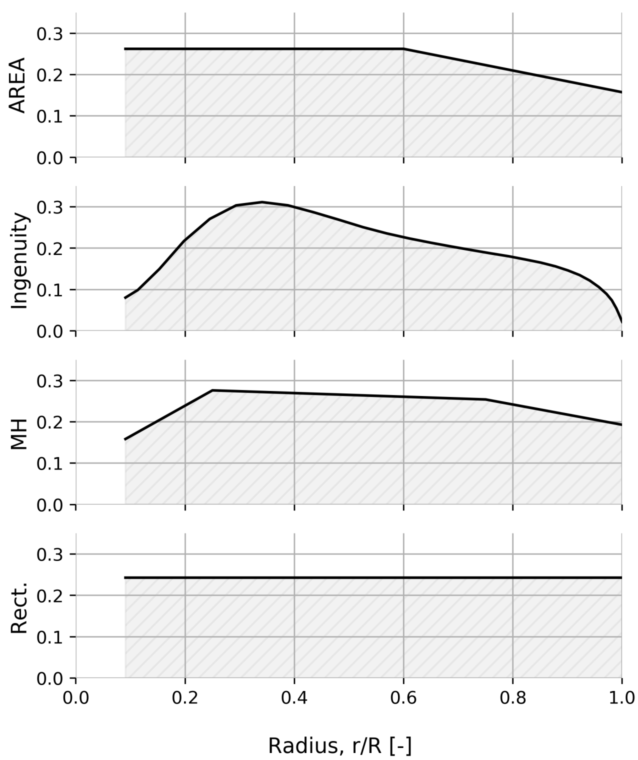

Figure 6: Baseline geometries, with MH and Ingenuity geometry taken from [7] and [9] respectively.

In order to allow comparability of different plan-forms, a commonly used metric is the thrust-based equivalent solidity, which is defined as shown in Equation 2 [5]. This allows a comparison of rotor power at a given thrust. All blade geometries were scaled in the chordwise direction to maintain their shape whilst adjusting their thrust-based equivalent solidity to be identical.

$$\sigma_e = 3 \cdot \int_0^1 \sigma r dr \tag{2}$$

To reduce sources of uncertainty and simplify the comparison, blade twist was neglected in this analysis, assuming that this does not affect the overall ranking of the geometries. This assumption was later reinforced by simulation data, as discussed in the chapter on twist.

The blades were analysed and compared concerning their power requirements over the course of the mission. The mission profile was divided into hover and cruise phases, with hover accounting for 10 % of the total mission duration. Power requirements for climb and descent were neglected. The results indicated that the Ingenuity rotor blade exhibited the lowest power demand in both hover and cruise phases. It decreased the power demand by about 8.2 %, thus outperforming the next best blade, the AREA configuration, by approximately 140 W. In contrast, performance differences among the other geometries were relatively small. Based on the performance advantage, the Ingenuity blade geometry was selected as the foundation for further optimization.

Parametrized Optimization

To improve the chord distribution for forward flight, the geometry was parametrized by way of four control points that are connected by a spline to preserve the profile's contour while enabling parametric modifications, see Figure 7. The location of the points was based on extreme points in the geometry, to control and constrain the maximum chord length. Additional points were added when necessary to approximate the geometry.

To investigate the performance sensitivity to geometric modifications, the control points were systematically varied in the chord wise direction by ±10 % of their original positions. As the thrust-based equivalent solidity and thus the blade area were still constraint, changes to one point necessitated compensatory adjustments to the others. This introduced interdependencies that complicate the identification of individual trends. For this reason, the usage of more points was also neglected. An additional constraint was introduced that set a minimum chord length for the outer section of the rotor blade. This was done to ensure its structural integrity.

This method yielded an optimized geometry. Figure 7 illustrates the variations resulting from modifications to each control point. These changes also impacted adjacent control points, highlighting the interconnectivity of

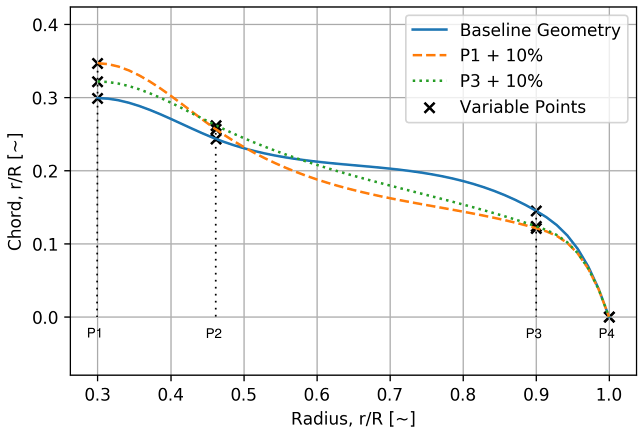

Figure 7: Comparison of optimized plan-forms to the baseline geometry.

the spline structure. The corresponding performance metrics are summarized in Tables 5 and 6.

Table 5: Required total power for different geometries in forward flight (40 m/s).

Case	Point 1 [W]	Point 2	Point 3
Baseline		1324.07	
+ 10 %	1294.81	1334.86	1367.09
- 10 %	1294.84	1314.43	1283.01
		Savings ΔP [%]	
+ 10 %	2.21	-0.81	-3.25
- 10 %	2.21	0.73	3.10

Table 6: Required total power for different geometries in hover.

Case	Point 1 [W]	Point 2	Point 3
Baseline		2692.23	
+ 10 %	2658.73	2693.84	2758.01
- 10 %	2728.75	2689.78	2622.13
		Savings ΔP [%]	
+ 10 %	1.24	-0.06	-2.44
- 10 %	-1.35	0.10	2.61

Both hover and cruise analyses revealed performance improvements with a shift of control point 3 towards lower chord lengths, resulting in approximately a 3.1 % reduction in power requirement. The final optimized blade geometry is presented in Figure 8.

Twist

The design process was carried out in parallel with the original geometry selection and revised again after the finalization of the outer geometry. Hover was analysed to see the different trend and adjust if necessary for the

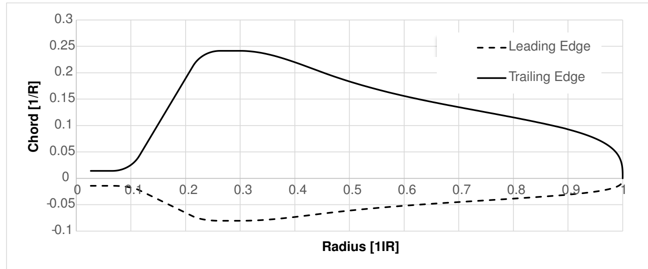

Figure 8: Finalized chord distribution.

10 % share of the mission. To ensure that the performance trends in the initial geometry are independent of the selected twist, a sweep was performed for all available geometries and then compared with each other, see Figure 10. It can be seen that the general trend from the geometry analysis in the previous chapters remains unchanged. There is no overlap of the curves at any time, so that the results of the geometry selection are still valid and the previously made assumption is correct.

For blades designed for hover, the ideal twist results in a hyperbolic curve [5]. As this leads to a more complicated manufacturing processes, a linear twist was considered instead. Although these do not correspond to the ideal, they approximate it well.

Twist was varied from 10 to -22 degrees. This range was selected based on experience and literature to capture the minimum performance. Figure 9 and 10 show the overall power requirement over twist for hover and cruise, respectively.

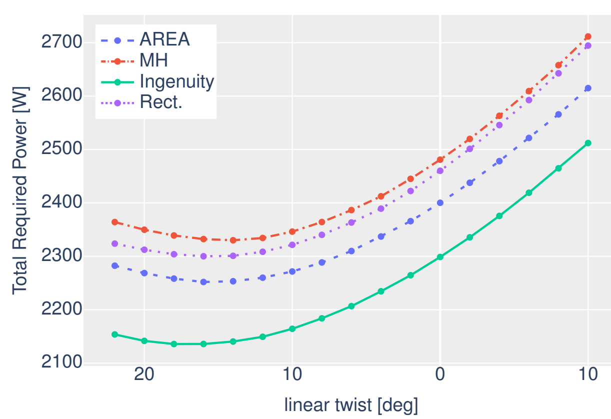

Figure 9: Power consumption over linear twist for different rotor blade geometries in hover.

It can be observed that both flight conditions result in different optima for twist. The optimum value for forward flight lies between -11 and -10 degrees, whereas

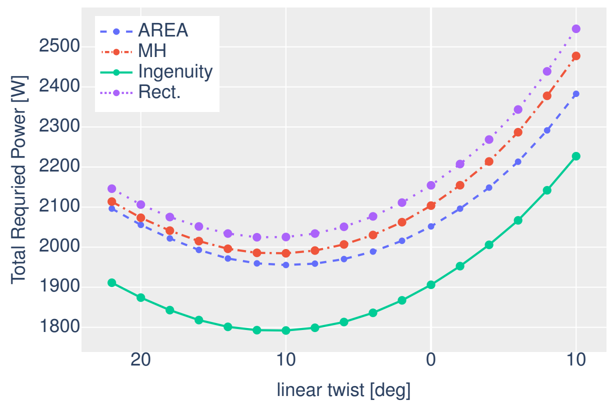

Figure 10: Power consumption over linear twist for different rotor blade geometries in forward flight.

the value for hover is between -18 degrees and -19 degrees. This is due to the superposition of the flow velocity and the rotational speed. The asymmetrical inflow in forward flight on the leading and trailing blade leads unfavourable inflow conditions for high twist, resulting in an overall lower ideal twist for forward flight. Due to the mission design, it was decided to use the optimum value for cruise. This was set at -10.5 degree. Following the geometry optimization and the adaptation of the elastic blade model, the investigations were repeated. These showed an earlier optimum in cruise, at -7.5 degrees linear twist, which was adopted for the rotor blade. A pre twist was introduced in the blade transition area. This ensures the transition between the untwisted blade root and the aerodynamically effective area with the specified twist. The pre twist was selected to allow a smooth transition and avoid and reduce stress peaks. The final result of the twist is shown in Figure 11.

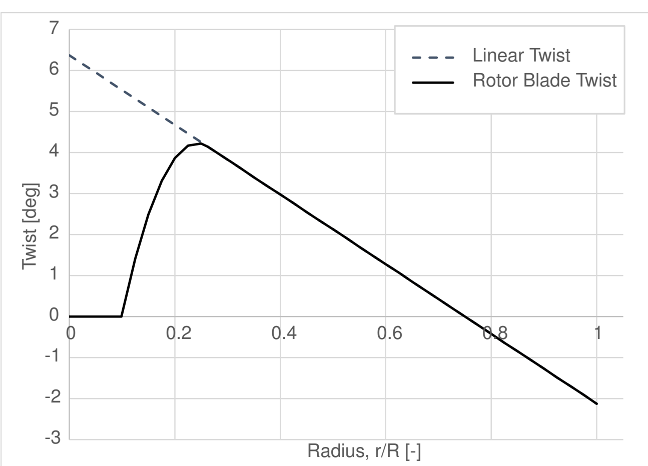

Figure 11: Blade twist final results.

Blade root

The blade root area represents the connection between the blade connection, which has a diameter of 43mm and the aerodynamically effective area. For the design, care must be taken to ensure that the geometry flows smoothly in order to prevent stress peaks in the ply structure. Excessive changes to the geometry can lead to problems for the tapering of the ply layers.

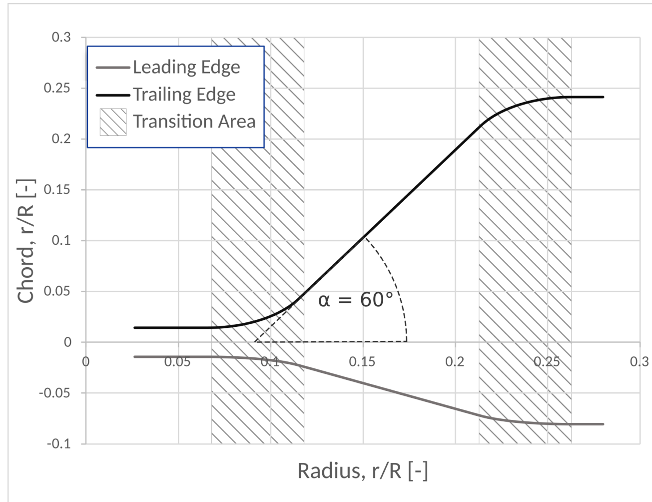

Figure 12: Blade root area.

Based on experience, a maximum angle of 60 degrees has been determined, which should not be exceeded. Since the chord optimization lead to an increased chord length of the inner blade area, the maximum angle of 60 degrees at the trailing edge (TE) was used to maximize the aerodynamic area. As the transition at the leading edge (LE) is smaller, it automatically fulfils this condition. In addition, an area of 10 cm in width was defined in each case to allow a smooth transition between the transition region and the other parts of the blade. This region, along with the final blade root design is depicted in Figure 12. With these boundary conditions, it follows that the transition area extends from R = 0.098 to R = 0.263.

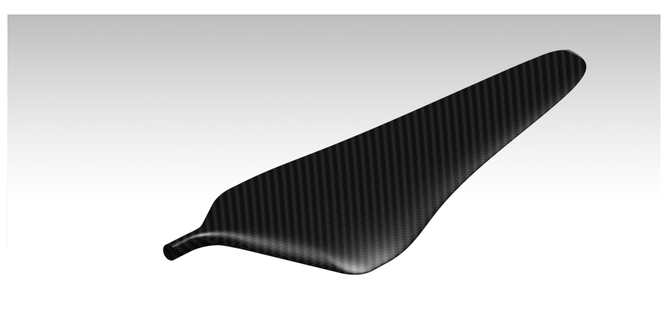

Figure 13: Rendering of the final rotor blade.

Comparison to hover optimized blade

The analysis showed, that the main influencing factor on the total required power in forward flight is the profile power. Therefore, the best results are achieved by reducing the chord length in the outer regions of the rotor blade that experience the highest velocities and produce the majority of drag. Due to the constraint of thrust-based equivalent solidity and thus blade area, this results in a larger chord length for the inner region of the blade to counteract the effect of the thin outer region. This is limited by the structural capabilities of the blade. Hence, it was decided to set a limit for the thinnest part of the rotor blade.

In comparison to the blade from Koning et al. [9], it can be observed, that the optimization caused a shift of the blade geometry towards the centre. This is the result of reducing the required profile power in forward flight, whereas the Ingenuity blade was optimized for hover. The shape itself did not change significantly, which is because the thinnest part of the rotor blade was limited to a minimum value.

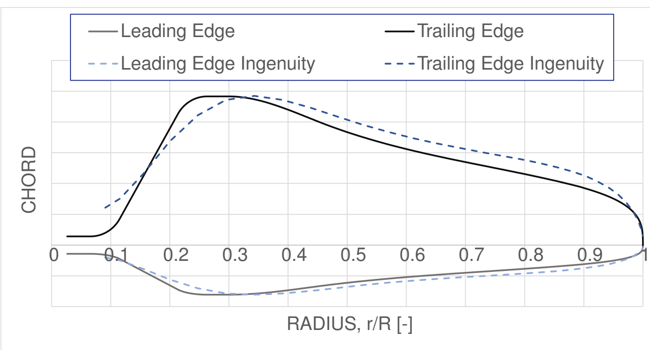

Figure 14: Qualitative comparison between the TUM rotor blade and Ingenuity rotor blade [9].

In terms of twist, the analysis shows that a lower linear twist if beneficial for the total required power. This trend could be observed throughout all tested blade geometries, as shown in Figures 9 and 10. Similar to the chord distribution, this is due to the profile power.

BLADE STRUCTURAL DESIGN

This section focuses on structural stability and eigenfrequency requirements. The ply lay-up of the rotor blades is beyond the scope of this study.

The rarefied Martian atmosphere not only poses a constraint in the aerodynamics of the rotor system but also its structural dynamics, as demonstrated by Fjeldheim et al. [2, 7]. On Earth, aerodynamic damping is the dominant mechanism for attenuating flap wise oscillations. Flapping motion induces a change in angle of attack, resulting in a lift force that acts opposite to the motion and thereby provides damping. Since this mechanism scales with air density, its effectiveness is considerably reduced under Martian conditions [2]. This is exemplified in the following equations:

$$\zeta = \frac{\gamma}{16\omega_0} \tag{3}$$

$$\gamma = \frac{\rho c C_{la} R^4}{l} \tag{4}$$

Here ζ is the non dimensional damping, γ is the blade Lock number, ρ is air density, c is the chord length and C_{la} the lift curve slope of the airfoil [2]. The consequence of these weakly damped flap modes is a greater susceptibility to dynamic instabilities. If control inputs excite frequencies near these natural modes, there is a risk of resonance, potentially leading to instability in the flight control system.

A mitigation strategy was proposed by Johnson et al. [7]. The paper suggests to increase the first regressive flap mode frequency to higher values as the bandwidth of the controller. This way, interference with control dynamics is avoided. Based on the data presented in [7], a bandwidth of requirement of 275 rad/s was set. This requirement was applied in the design of a proposed hexacopter concept with a rotor radius of 0.64 m and a rotational speed of 2435 rpm. For this configuration, a blade flap frequency of 1.1 /rev was sufficient to meet the criterion [7].

The proposed VaMEx Mars Helicopter features a larger rotor radius, resulting in a lower nominal rotational speed of 1162 rpm. To satisfy the same eigenfrequency constraint, the first flap wise frequency must therefore exceed 3.26 /rev. Achieving this target necessitates substantially stiffer blades, which in turn leads to an increase in blade mass and presents additional design challenges.

Based on the findings of this evaluation, a change towards a smaller blade radius is suggested for future rotorcraft.

CONCLUSIONS

In this study, the VaMEx initiative is introduced, focusing on the design of a rotor system and rotor blades for an unmanned aerial vehicle capable of carrying a 2.2 kg payload over a range of 30 km. The primary design point corresponds to cruise flight at a velocity of 40 m/s.

An aeromechanical rotor model of the VaMEx Mars Helicopter was developed using CAMRAD II and validated against experimental data from the JPL-SS rotor tests, as well as through assessment of physical consistency. The model demonstrated good agreement with the reference data and was successfully scaled to a rotor radius of 1.52 m. While the model exhibited generally good numerical stability, instabilities were observed at high levels of geometric discretisation.

Based on this validated model, a preliminary automated optimisation framework was proposed, integrating CAMRAD II and SONATA, a preprocessor for parametric composite rotor blade cross-sections. Although the approach was conceptually promising, the high sensitivity of the rotor model to geometric perturbations rendered it impractical for the current study. Consequently, future work will investigate this optimisation strategy under more conventional rotor blade configurations and atmospheric conditions.

Instead, a manual design approach was adopted. The CLF5605 airfoil, previously used on the Mars Helicopter, was selected due to its superior structural stiffness, despite the potentially higher aerodynamic efficiency of cambered plate airfoils. After evaluating five blade geometries, the Mars Helicopter blade plan-form was chosen as the baseline for subsequent optimisation targeting forward flight performance.

The rotor blade geometry was parametrised, and a sensitivity analysis was conducted to assess the influence of geometric variations. Results indicated that profile power is the dominant contributor to overall power consumption in forward flight. Consequently, chord length was reduced toward the blade tips and increased near the root. A parametric sweep over linear twist distributions identified an optimal twist of -7.5 degrees over the rotor span.

Structural analysis revealed challenges in achieving the desired first flap wise eigenfrequencies, primarily due to the low rotational speed and the high stiffness requirements. Therefore, transitioning to a configuration with smaller rotor blades is considered a more feasible solution for future development.

Author contact: Stefan Hönes stefan.hoenes@tum.de
Ilkay Yavrucuk ilkay.yavrucuk@tum.de

ACKNOWLEDGMENTS

This research project is part of the collaborative research project VaMEx and was funded by the Federal Ministry for Economics and Climate Action. The project partners are INVENT GmbH and the Technical University of Munich (TUM), and the project is led by the German Aerospace Center (DLR).

Gefördert durch:

Bundesministerium
für Wirtschaft
und Klimaschutz

aufgrund eines Beschlusses
des Deutschen Bundestages

*

References

1. VaMEx Initiative – Valles Marineris Explorer.

2. H. Fj, L. Young, B. Allan, B. Mettler, and M. S. Martin. Flight Dynamics of a Mars Helicopter. volume 43, 2017.

3. F. Forget, F. Hourdin, R. Fournier, C. Hourdin, O. Talagrand, M. Collins, S. R. Lewis, P. L. Read, and J. Huot. Improved general circulation models of the Martian atmosphere from the surface to above 80 km. *Journal of Geophysical Research: Planets*, 104(E10):24155–24175, Oct. 1999.

4. W. Johnson. CAMRAD II - Comprehensive Analytical Model of Rotorcraft Aerodynamics and Dynamics.

5. W. Johnson. *Helicopter Theory*. 1980.

6. W. Johnson and M. Field. NDARC NASA Design and Analysis of Rotorcraft. 2009.

7. W. Johnson, S. Withrow-Maser, L. Young, C. Malpica, W. J. F. Koning, M. Fehler, A. Tuano, A. Chan, A. Datta, C. Chi, R. Lumba, D. Escobar, J. Balaram, T. Tzanetos, and H. Fj. Mars Science Helicopter Conceptual Design. Technical Memorandum ARC-E-DAA-TN78199, Ames Research Center, 2020.

8. W. J. F. Koning. Airfoil Selection for Mars Rotor Applications. Contractor Report (CR) ARC-E-DAA-TN70055, Ames Research Center, 2019.

9. W. J. F. Koning and M. Dominguez. Mars Helicopter Ingenuity Rotor Geometry. Technical Memorandum, Ames Research Center, 2024.

10. W. J. F. Koning, W. Johnson, and B. G. Allan. Generation of Mars Helicopter Rotor Model for Comprehensive Analyses.

11. W. J. F. Koning, W. Johnson, and H. F. Grip. Improved Mars Helicopter Aerodynamic Rotor Model for Comprehensive Analyses. *AIAA Journal*, 57(9):3969–3979, Sept. 2019.

12. NASA Ames Research Center, W. J., E. Romander, and W. Johnson. Low Reynolds Number Airfoil Evaluation for the Mars Helicopter Rotor. In *Proceedings of the Vertical Flight Society 74th Annual Forum*, pages 1–17, Phoenix, Arizona, May 2018. The Vertical Flight Society.

13. V. A. Petrovych. The Atmosphere of Mars. In *Proceedings of VI International Scientific and Practical Conference. Scientific research in the modern world.* Perfect Publishing, Chapter 45, 2023.

14. D. R. Williams. *Mars Fact Sheet*. NSSDCA.

15. V. Zappek, M. Rinker, L. Daxer, and M. Hajek. Configuration Analysis of a High Range Mars Scout UAV.

CLASSIFICATION & COPYRIGHT